Chapter 7

Geometrical Optics

Concepts from geometrical optics—rays and all that—have occasionally intruded upon our discussions in preceding chapters, even in contexts where they were not strictly applicable. In spite of its limitations, geometrical optics is a simple and intuitively appealing approximate theory which need not be abandoned simply because the exact theory is at hand. In addition to its role in guiding intuition, geometrical optics can often provide quantitative answers to small-particle problems which are sufficiently accurate for many purposes, particularly when one soberly considers the accuracy with which many measurements can be made. In this chapter, therefore, we consider scattering and absorption by spheres within the framework of geometrical optics and compare these results with those of the exact theory. No book on light scattering by small particles would be complete without discussing the rainbow, the main features of which are quite adequately explained with simple geometrical optics; this then leads into atmospheric optical phenomena involving nonspherical particles for which there are no exact theories.

7.1 ABSORPTION AND SCATTERING CROSS SECTIONS

In this section we derive an approximate expression for the absorption cross section of a large weakly absorbing sphere. We assume that the incident plane wave can be subdivided into a large number of rays the behavior of which at interfaces is governed by the Fresnel equations and Snell's law (Section 2.7). A representative ray incident on the sphere at an angle Θ_i is shown in Fig. 7.1. At point 1 on the surface of the sphere the incident ray is divided into externally reflected and internally transmitted rays; these lie in the plane of incidence, which is determined by the normal to the sphere and the direction of the incident ray. If the polar coordinates of point 1 are (a, Θ_i, ϕ), the plane of incidence is the plane ϕ = constant. At point 2 the transmitted ray encounters another boundary and therefore is partially reflected and partially transmitted. In a like manner we can follow the path of the rays within the sphere, a path that does not deviate outside the plane of incidence. At each point where a ray encounters a boundary it is partially reflected internally and partially transmitted into the surrounding medium. On physical grounds we know that the absorption cross section cannot depend on the polarization of the incident

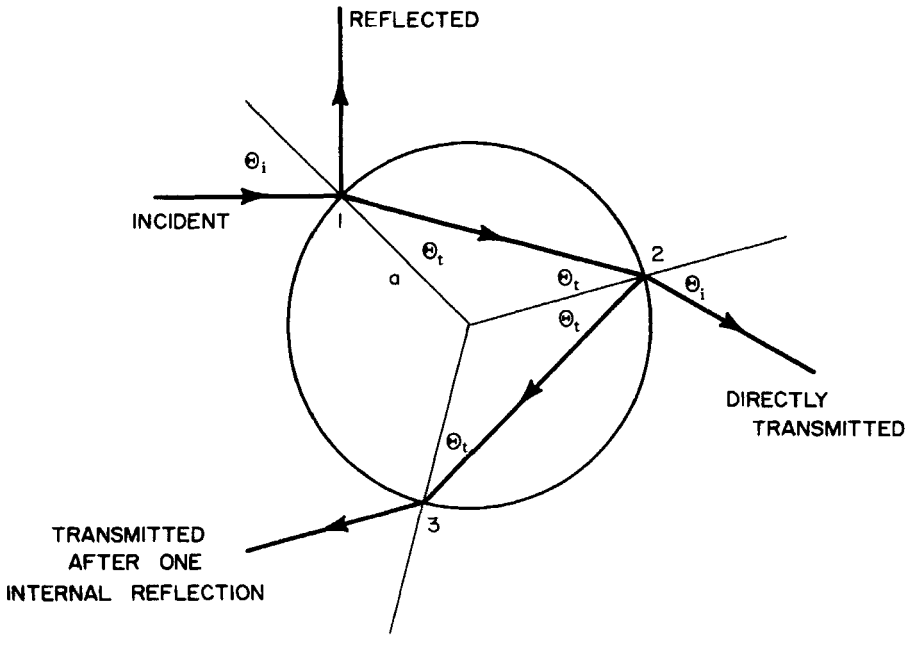

Figure 7.1 Ray-tracing diagram.

beam, which, for convenience, we may choose to be x-polarized. The components of the incident electric field parallel and perpendicular to the plane of incidence are $E_{\|i} = E_i \cos\phi$ and $E_{\perp i} = E_i \sin\phi$. We showed in Section 2.7 that these two components are reflected and transmitted independently of each other; therefore, we may consider each component in turn.

Let us first consider the component parallel to the plane of incidence. We assume that the imaginary part of the complex refractive index $m = n + ik$ of the sphere relative to the surrounding medium is small compared with the real part; therefore, the (real) angle of refraction Θ_t is to good approximation given by $\sin\Theta_t = \sin\Theta_i/m$. We may also ignore the imaginary part of m in the Fresnel equations (2.67)–(2.70). At point 1 the amplitude $E_{\|t}$ of the transmitted field is $\tilde{t}_{\|}(\Theta_i, n)E_{\|i}$, where the transmission coefficient $\tilde{t}_{\|}$ is given by (2.68). Therefore, the amount of energy that is transmitted through an element of area at 1 is

$$\frac{\mathrm{Re}\{N_1\}\cos\Theta_t |E_{\|t}|^2 a^2 \sin\Theta_i \, d\Theta_i \, d\phi}{2Z_0},$$

where $Z_0 = \sqrt{\mu_0/\varepsilon_0}$ is the impedance of free space and N_1 is the refractive index of the sphere. The incident irradiance $I_{\|i}$ is $N|E_{\|i}|^2/2Z_0$, where N is the (real) refractive index of the surrounding medium. The expression above may

be written more concisely as

$$T_{\|}(\Theta_i, n) I_{\|i} \cos\Theta_t a^2 \sin\Theta_i \, d\Theta_i \, d\phi,$$

where the *transmittance* is defined as

$$T_{\|}(\Theta_i, n) = \frac{n|\tilde{t}_{\|}(\Theta_i, n)|^2 \cos\Theta_t}{\cos\Theta_i}.$$

A fraction $1 - e^{-\alpha\xi}$ of the transmitted energy at 1 is absorbed as the ray traverses a path length $\xi = 2a\sqrt{n^2 - \sin^2\Theta_i}/n$ between points 1 and 2, where α is the absorption coefficient of the sphere. The amplitude of the reflected field at 2 is

$$E_{\|i} \tilde{t}_{\|}(\Theta_i, n) e^{-\alpha\xi/2} \tilde{r}_{\|}\left(\Theta_t, \frac{1}{n}\right),$$

where $\tilde{r}_{\|}$ is the reflection coefficient; note that at 2 the angle of incidence is Θ_t and the relative refractive index is $1/n$. This reflected ray traverses the same path length ξ between 2 and 3; in so doing, an amount of energy

$$I_{\|i} T_{\|i}(\Theta_i, n) R_{\|}\left(\Theta_t, \frac{1}{n}\right) e^{-\alpha\xi} a^2 \cos\Theta_i \sin\Theta_i \, d\Theta_i \, d\phi (1 - e^{-\alpha\xi})$$

is absorbed in the sphere, where the reflectance $R_{\|}$ is $|\tilde{r}_{\|}|^2$. It is evident from the expression above that the amount of energy deposited by each successive internally reflected ray is $R_{\|} e^{-\alpha\xi}$ times that deposited by its predecessor.

If the incident field component is perpendicular to the plane of incidence, all the expressions for reflected, transmitted, and absorbed light are identical in form with those in the preceding paragraph; we need merely substitute $R_{\perp}$ and $T_{\perp}$ for $R_{\|}$ and $T_{\|}$.

The total energy W_{abs} absorbed in the sphere is obtained by summing the energy deposited by all internal rays for both components of polarization and a given incident ray and then integrating over all incident rays (i.e., all angles of incidence between 0 and $\pi/2$). The result is

$$W_{\text{abs}} = I_i 2\pi a^2 \int_0^{\pi/2} \left\{ T(\Theta_i, n) \sum_{j=0}^{\infty} \left[R(\Theta_t, 1/n) e^{-\alpha\xi} \right]^j \times (1 - e^{-\alpha\xi}) \cos\Theta_i \sin\Theta_i \, d\Theta_i \right\}, \tag{7.1}$$

where T and R are the transmittance and reflectance for unpolarized incident light

$$T = \tfrac{1}{2}(T_{\|} + T_{\perp}), \qquad R = \tfrac{1}{2}(R_{\|} + R_{\perp}),$$

and $I_i = I_{\|i} + I_{\perp i}$ is the total incident irradiance. The infinite series in (7.1) is readily summed:

$$\sum_{j=0}^{\infty} \left[R\left(\Theta_t, \frac{1}{n}\right) e^{-\alpha\xi} \right]^j = \frac{1}{1 - R(\Theta_t, 1/n) e^{-\alpha\xi}}.$$

Conservation of energy at boundaries requires that

$$R + T = 1,$$

and the reciprocal relations

$$R\left(\Theta_t, \frac{1}{n}\right) = R(\Theta_i, n), \qquad T\left(\Theta_t, \frac{1}{n}\right) = T(\Theta_i, n)$$

follow from the Fresnel formulas.

Up to this point we have only assumed that $k \ll n$; subject to this restriction and, of course, the assumption that geometrical optics combined with the Fresnel formulas is a good approximation, (7.1) is completely general. Let us further assume that the sphere is sufficiently weakly absorbing that $2a\alpha \ll 1$; with this assumption

$$1 - e^{-\alpha\xi} \simeq \alpha\xi, \qquad \frac{1}{1 - Re^{-\alpha\xi}} \simeq \frac{1}{T}$$

and (7.1) becomes

$$W_{\text{abs}} = \frac{4\pi a^3 \alpha}{n} I_i \int_0^{\pi/2} \cos\Theta_i \sqrt{n^2 - \sin^2\Theta_i} \sin\Theta_i \, d\Theta_i,$$

which can be integrated to yield the absorption cross section $C_{\text{abs}} = W_{\text{abs}}/I_i$:

$$C_{\text{abs}} = \frac{4}{3}\pi a^3 \frac{\alpha}{n}\left[n^3 - (n^2 - 1)^{3/2}\right]. \tag{7.2}$$

Note that the absorption cross section of a weakly absorbing sphere, like that of a particle small compared with the wavelength (Chapter 5), is, in the geometrical optics limit, proportional to its volume. This proportionality does not hold, however, for indefinitely large particle radius. Energy is absorbed primarily in the outer layer of a highly absorbing sphere (i.e., $2a\alpha \gg 1$), and the interior of such a sphere plays no role in the absorption process. As the radius increases, therefore, the absorption cross section becomes proportional to *area* instead of *volume*.

Equation (7.2) was derived under the implicit assumption that the phase of the light could be ignored. In a like manner, we derived the transmittance of a slab in Section 2.8 by considering only irradiances and showed that the

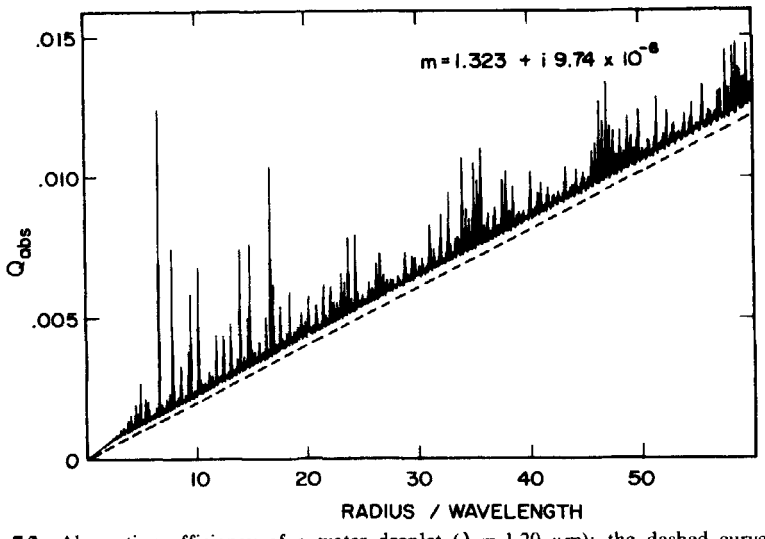

Figure 7.2 Absorption efficiency of a water droplet ($\lambda = 1.20\ \mu m$); the dashed curve is the geometrical optics approximation (7.2).

resulting expression is valid under conditions for which interference effects are obliterated by sufficient departure from monochromaticity of the incident beam or planarity of the slab. C_{abs} in (7.2) should therefore be interpreted as the average cross section of a collection of particles with a distribution of radii sufficiently wide that interference effects may be neglected.

To assess the accuracy of this approximation, therefore, we should compare its predictions with exact calculations for a size distribution, although this is not really necessary. Accordingly, Fig. 7.2 shows the absorption efficiency of a single water droplet in air at a wavelength of 1.20 μm; the optical constants are taken from Irvine and Pollack (1968). If we ignore the extremely narrow peaks (ripple structure), which are smoothed by averaging over a distribution of radii (see Section 11.3, particularly Fig. 11.6), there is generally good agreement between the exact and approximate theories: the absorption efficiency increases linearly with radius in accordance with (7.2).

In collections of naturally occurring particles, such as water droplets in a cumulus cloud, there usually will be a considerable dispersion of radii. This will be true even in laboratory experiments unless special care is taken. For such applications, (7.2) is expected to be a good approximation provided, of course, that the particles satisfy the conditions under which it was derived: they must be large and weakly absorbing. For example, (7.2) has been incorporated in radiative transfer calculations for snow (Bohren and Barkstrom, 1974) and clouds (Twomey and Bohren, 1980).

In Fig. 7.3 we show the absorption efficiency for a water droplet at a wavelength (1.45 μm) where water is considerably more absorbing than at 1.20

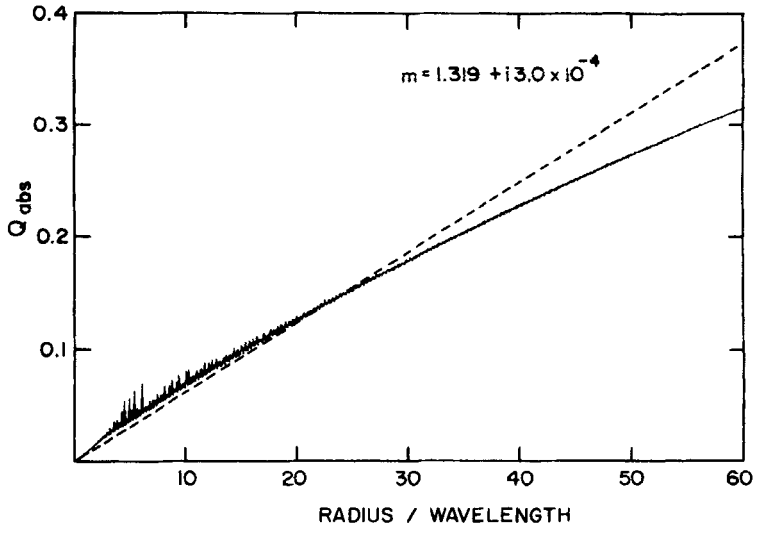

Figure 7.3 Absorption efficiency of a water droplet ($\lambda = 1.45$ μm); the dashed curve is the geometrical optics approximation (7.2).

μm. The agreement between exact and approximate theories begins to systematically worsen for radii such that $a\alpha > 0.1$; this gives us an approximate criterion for the range of validity of (7.2). As the particle radius increases, the absorption efficiency approaches a limiting value, which we shall discuss in the following paragraphs.

7.1.1 Asymptotic Absorption and Scattering Efficiencies

The total energy W_{sca} scattered by a large sphere may, to good approximation, be written as the sum of diffracted, reflected, and transmitted components:

$$W_{sca} = W_{diff} + W_{refl} + W_{tr}, \tag{7.3}$$

where the transmitted energy W_{tr} may be further subdivided into a directly transmitted component, a component transmitted after one internal reflection, and so on (see Fig. 7.1):

$$W_{tr} = \sum_{j=1}^{\infty} W_{tr,j}. \tag{7.4}$$

The externally reflected energy is given by

$$W_{refl} = I_i 2\pi a^2 \int_0^{\pi/2} R(\Theta_i)\cos\Theta_i \sin\Theta_i \, d\Theta_i,$$

and it is natural to define the *reflection cross section* C_{refl} as W_{refl}/I_i; the *reflection efficiency* is therefore

$$Q_{\text{refl}} = 2\int_0^{\pi/2} R(\Theta_i)\cos\Theta_i \sin\Theta_i \, d\Theta_i. \tag{7.5}$$

All the light that enters a sufficiently large absorbing sphere ($a\alpha \gg 1$) will be absorbed; none of the unreflected light will be transmitted. We showed in Chapter 4 that the diffraction cross section of a large sphere is πa^2; thus, we might expect the limiting value of the scattering efficiency to be

$$\lim_{x\to\infty} Q_{\text{sca}} = 1 + Q_{\text{refl}}, \tag{7.6}$$

provided that $k \neq 0$. However, the asymptotic value (7.6) for the scattering efficiency is not universally accepted. Herman (1962) suggested that the scattering efficiency should approach the limit $1 + R(0°)$, where $R(0°) = |(m - 1)/(m + 1)|^2$ is the reflectance at normal incidence, on the grounds that a sphere becomes a planar surface as the size parameter x increases without limit. Deirmendjian (1969, pp. 34–41), however, argued that this conjecture is incorrect and that (7.6) is the proper limiting value. Nevertheless, Chýlek (1975) constructed a mathematical proof that $1 + R(0°)$ is the limiting value for Q_{sca}. Bohren and Herman (1979) subsequently concluded, on the basis of computations and physical arguments, that Chýlek's proof is in error, although they were not able to uncover the exact nature of this error; this was later done by Acquista et al. (1980).

To support the correctness of (7.6) we show in Fig. 7.4 Q_{sca} as a function of $1/x$, where $x = 2\pi a/\lambda$, computed from the exact theory for a sphere with refractive index $1.3 + i0.1$; for comparison, the limiting values $1 + R(0°)$ and $1 + Q_{\text{refl}}$ are also shown. It is clear from this figure that $1 + Q_{\text{refl}}$ is an increasingly better approximation to Q_{sca} as x increases. On physical grounds it is implausible that scalar diffraction theory and geometrical optics is a good approximation for a large range of the size parameter but then ceases to be so as x increases beyond some particular value; if the computed values are to reach the limit $1 + R(0°)$, however, this is what is required (see Fig. 7.4). At what value of x does (7.6) cease to be a good approximation, and what is the physical reason for such a value? We know of no such reason. Therefore, we conclude that $1 + R(0°)$ is not the asymptotic efficiency. A sphere is always a sphere and cannot be transformed into a slab by increasing its radius indefinitely, although at any point on its surface, a sphere can be considered *locally* planar to a degree of accuracy that increases with increasing radius. Nevertheless, even for an arbitrarily large sphere, the angle of incidence is a function of position and cannot be the same at all points.

We also showed in Chapter 4 that $\lim_{x\to\infty} Q_{\text{ext}} = 2$; this, together with (7.6), implies that

$$\lim_{x\to\infty} Q_{\text{abs}} = 1 - Q_{\text{refl}}. \tag{7.7}$$

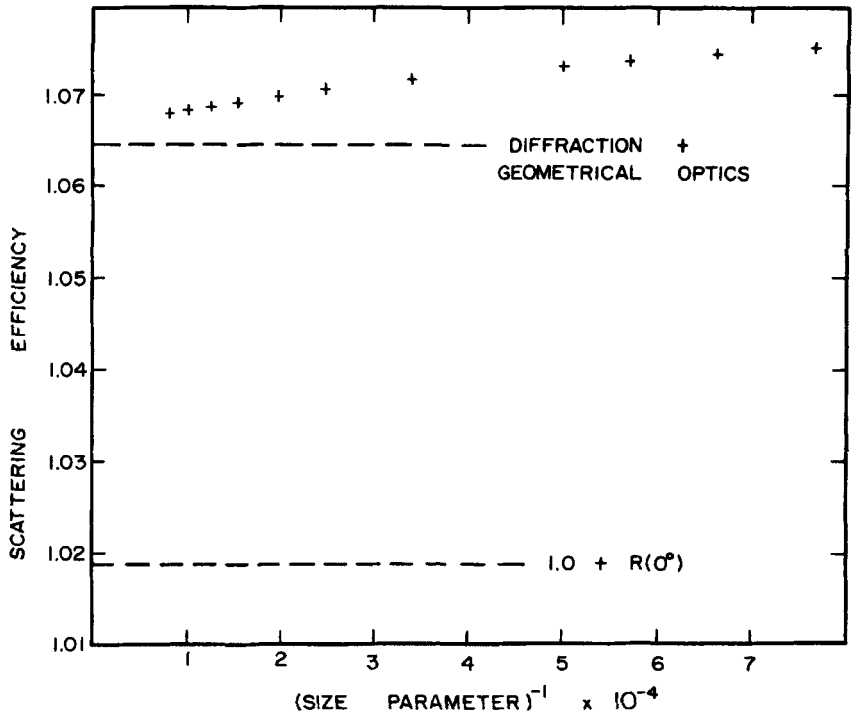

Figure 7.4 The crosses are computed from Mie theory. Scalar diffraction theory and geometrical optics predict the limiting value 1.067. From Bohren and Herman, 1979.

The physical interpretation of (7.7) is straightforward: all the geometrically incident light that is not externally reflected enters the sphere and is eventually absorbed provided, of course, that the absorptive part of the refractive index is not identically zero. As long as there is some absorption, no matter how small, all the transmitted light will be absorbed in the sphere for sufficiently large radius a.

7.1.2 Reflection and Transmission Efficiencies for a Nonabsorbing Sphere

It follows from (7.3) that the scattering efficiency of a large sphere can be written

$$Q_{\text{sca}} = Q_{\text{diff}} + Q_{\text{refl}} + Q_{\text{tr}},$$

where Q_{diff}, the diffraction efficiency, is unity and Q_{refl}, the (external) reflection efficiency, is given by (7.5). Furthermore, from (7.4), the transmission

Table 7.1 Reflection and Transmission Efficiencies for a Nonabsorbing Sphere with $m = 1.33$

Q_{refl}	$Q_{\text{tr},1}$	$Q_{\text{tr},2}$	$Q_{\text{tr},3}$	$Q_{\text{tr},4}$
0.06593	0.88451	0.04033	0.00607	0.00171
$Q_{\text{refl}} + Q_{\text{tr},1} + Q_{\text{tr},2} + Q_{\text{tr},3} + Q_{\text{tr},4} = 0.99855$				

efficiency Q_{tr} can be written as a series

$$Q_{\text{tr}} = \sum_{j=1}^{\infty} Q_{\text{tr},j},$$

where $Q_{\text{tr},j}$ is the contribution to the total transmission efficiency from rays that have undergone $j - 1$ internal reflections (see Fig. 7.1).

The extinction efficiency of a *nonabsorbing* sphere is equal to its scattering efficiency; for such a sphere, provided that it is sufficiently large, it necessarily follows that $Q_{\text{refl}} + Q_{\text{tr}} = 1$ and

$$Q_{\text{tr},j} = 2\int_0^{\pi/2} T_j(\Theta_i)\cos\Theta_i \sin\Theta_i \, d\Theta_i,$$

$$T_j = \tfrac{1}{2}\left(R_{\parallel}^{j-1}T_{\parallel}^2 + R_{\perp}^{j-1}T_{\perp}^2\right). \tag{7.8}$$

In Table 7.1 we give Q_{refl} and the first four terms in the series for Q_{tr}; the refractive index of the sphere is 1.33, which corresponds to a water droplet at visible wavelengths. One sometimes encounters the assertion that scattering by large transparent particles is the result of reflection at the particle–medium interface; indeed, reflection is sometimes used as a synonym for scattering. It should be clear from Table 7.1, however, that this is very much wide of the mark: only about 6.6% of the light scattered by a large water droplet—exclusive of that diffracted, which is confined to a narrow set of angles about the forward direction—is the result of reflection; most of the scattered light—over 88%—can be attributed to rays that are bent on a single traverse of the droplet, the directly transmitted rays.

7.2 ANGULAR DISTRIBUTION OF THE SCATTERED LIGHT: RAINBOW ANGLES

Externally reflected rays, directly transmitted rays, rays transmitted after undergoing one or more internal reflections, all can contribute to the light scattered into a unit solid angle about a particular direction. The incident rays are evenly spaced; but after reflection and transmission they can be concentrated in particular directions, much like the concentration or focusing of rays by a lens.

As in the preceding section, we may imagine that a ray incident on a sphere at an angle Θ_i between 0 and $\pi/2$ is decomposed into an infinite number of rays of varying strengths because of interaction with the sphere. For a given Θ_i the angle θ in which a particular type of ray is scattered can be determined from Fig. 7.1 by elementary trigonometry:

$$\begin{aligned}
&\theta = \pi - 2\Theta_i && \textit{externally reflected} \\
&\theta = 2\Theta_i - 2\Theta_t && \textit{directly transmitted} \\
&\theta = 2(n_r + 1)\Theta_t - 2\Theta_i && \textit{transmitted after } n_r \textit{ internal reflections; } n_r \textit{ even} \\
&\theta = 2\Theta_i - 2(n_r + 1)\Theta_t + \pi && \textit{transmitted after } n_r \textit{ internal reflections; } n_r \textit{ odd}
\end{aligned} \tag{7.9}$$

where $n_r = 1, 2, \ldots$ and $m \sin \Theta_t = \sin \Theta_i$; we have also assumed that $1 < m < 2$ and done some fiddling to ensure that θ lies between 0 and π.

The light incident on an element of area $a^2 \sin \Theta_i \, d\Theta_i \, d\phi$ of the sphere is scattered into a solid angle $\sin \theta \, d\theta \, d\phi$ about the direction (θ, ϕ). The contribution to this scattered light from rays of the kth type is of the form

$$F_k(\Theta_i, \phi) \cos \Theta_i \sin \Theta_i \, d\Theta_i \, d\phi, \tag{7.10}$$

where we have folded into F_k the sphere radius, the incident irradiance, and the various reflectances and transmittances appropriate to each type of ray. Because we are primarily interested in singularities in the scattering diagram predicted by geometrical optics rather than its precise mathematical form, we shall not need explicit expressions for F_k; suffice it to say that F_k is finite for all angles of incidence. It follows from (7.10) that the light scattered into a unit solid angle about (θ, ϕ)—the *intensity* in modern terminology—is the sum over terms of the form

$$F_k(\Theta_i, \phi) \frac{\cos \Theta_i \sin \Theta_i}{\sin \theta} \frac{d\Theta_i}{d\theta},$$

where $(d\Theta_i/d\theta)$ is obtained from (7.9); the factor $(\cos \Theta_i \sin \Theta_i)/\sin \theta$ is finite for all angles of incidence. For externally reflected rays $d\Theta_i/d\theta$ is merely a constant; but for the various transmitted rays we have

$$\frac{d\Theta_i}{d\theta} = \frac{\pm 1}{2 - 2(n_r + 1)\dfrac{d\Theta_t}{d\Theta_i}}, \tag{7.11}$$

$$\frac{d\Theta_t}{d\Theta_i} = \frac{\cos \Theta_i}{\sqrt{m^2 - \sin^2 \Theta_i}}, \tag{7.12}$$

where $n_r = 0, 1, 2, \ldots$. Therefore, according to geometrical optics, the scattered intensity is infinite at those scattering angles where one of the conditions

$$\frac{d\Theta_t}{d\Theta_i} = \frac{1}{n_r + 1} \qquad (n_r = 0, 1, 2, \ldots) \tag{7.13}$$

is satisfied. It is clear that (7.13) is not satisfied for the directly transmitted ray ($n_r = 0$), but can be satisfied for the various internally reflected rays. Equations (7.12) and (7.13) can be combined to give

$$\cos\Theta_i = \sqrt{\frac{m^2 - 1}{n_r(n_r + 2)}}\,.$$

The scattering angles at which the intensity is infinite according to geometrical optics are called *rainbow angles*: the *primary* rainbow corresponds to rays that have undergone a single internal reflection; the *secondary* rainbow to rays that have undergone two internal reflections; the *tertiary* rainbow to rays that have undergone three internal reflections; and so on.

Although the scattered intensity can be quite large, it cannot be infinite at any angle; consequently, geometrical optics is strictly incorrect. This is similar to the result from geometrical optics that the intensity at the focal point of a lens, through which passes a finite amount of light, is infinite. Such singularities in the geometrical optics light field are called *caustics*. Rainbows are therefore caustics.

Although geometrical optics does not correctly give the magnitude of strong intensity maxima in the scattering diagram of large transparent spheres, it can give their positions to good approximation. This is readily verified by observations on rainbows formed by water droplets illuminated by the sun. The condition for the primary rainbow is

$$\cos\Theta_i = \sqrt{\frac{m^2 - 1}{3}} \tag{7.14}$$

and that for the secondary rainbow is

$$\cos\Theta_i = \sqrt{\frac{m^2 - 1}{8}}\,; \tag{7.15}$$

the corresponding scattering angles are determined from (7.9). Note that there cannot be a primary rainbow angle if m is greater than 2.

If we take $m = 1.333$ as the average refractive index of water over the visible spectrum, we obtain

$\theta = 137.9°$ *primary rainbow*

$\theta = 129.1°$ *secondary rainbow*

Rainbows of order higher than the second are not observed in the atmosphere;

they fade into the background illumination. In the laboratory, however, it is possible to observe higher-order rainbows and, moreover, to use liquids other than water. The highest-order rainbow ever observed has so far escaped the attention of the compilers of *Guinness' Book of World Records*, but in a paper highly recommended to rainbow aficionados, Walker (1976) has described observations of, among other things, a seventeenth-order corn syrup bow.

Rainbows may be seen during showers when the sun is behind the observer; the direction of the sunlight determines the forward direction (or line of sight). The angular positions of the primary and secondary rainbows relative to the observer's line of sight are $180° - 137.9° = 42.1°$ and $180° - 129.1° = 50.9°$, respectively. The fraction of the total rainbow that can be seen depends on the solar elevation. When the sun is greater than about 51° above the horizon, no rainbow can be seen even though conditions are otherwise favorable. On the other hand, the complete rainbow—one that forms a complete circle—may be seen from an airplane.

Were it not for dispersion—the refractive index depends upon wavelength— the aesthetic appeal of rainbows would be greatly diminished. Indeed, the word "rainbow" used in everyday speech evokes images of a profusion of colors—the colors of the rainbow—rather than just an intensely bright arc in the sky. If we take $m = 1.343$ as the refractive index of "violet" light ($\lambda \simeq 0.4$ μm) and $m = 1.331$ as the refractive index of "red" light ($\lambda \simeq 0.65$ μm) (Irvine and Pollack, 1968), then the angular widths of the primary and secondary rainbows are about 1.7° and 3.1°, respectively.

Rainbow angles correspond to those angles of incidence at which the denominator of (7.11) vanishes; because $d\theta/d\Theta_i = 1/(d\Theta_i/d\theta)$, this in turn implies that for given n_r the rainbow angles correspond to *extrema* of the function $\theta(\Theta_i)$. The nature of these extrema are determined by the sign of $d^2\theta/d\Theta_i^2$: minima for odd n_r, maxima for even n_r. Thus, the primary rainbow angle 137.9° corresponds to a *minimum* of θ; the secondary rainbow angle 129.1° corresponds to a *maximum* of θ. Consequently, there is a dark band, *Alexander's dark band*, about 9° wide between the primary and secondary rainbows. Note, however, that both rainbow angles are angles of *minimum deviation*: they correspond to rays that have suffered the least *total* deviation.

Geometrical optics successfully explains the major features of the rainbow: the angular positions of the primary and secondary bows, their widths, color separation, and Alexander's dark band. As might be expected, it cannot explain all the observed features. According to geometrical optics, all rainbows are equal under conditions of similar illumination: the size distribution of droplets is irrelevant. But it is a matter of common experience that some rainbows are more vivid than others. *Supernumerary bows* (i.e., ones that should not exist according to geometrical optics) are sometimes observed below the primary bow; these require invoking interference arguments for their explanation. All this is beyond the scope of geometrical optics. For more details about rainbows we direct the reader to the list of references at the end of this chapter.

7.3 SCATTERING BY PRISMS: ICE CRYSTAL HALOES

It might naively be supposed that a collection of nonspherical particles, if randomly oriented, is equivalent to a suitably chosen collection of spheres. Evidence to the contrary is freely available—more frequently than is commonly thought—to all who would look toward the sun through thin veils of high cirrus clouds and observe the various halo phenomena that owe their existence to scattering by ice crystals. By simple geometrical arguments, similar to those in the preceding section, we can acquire an understanding of many of the features of ice crystal haloes and their associated arcs.

Consider a transparent triangular prism with refractive index m and vertex angle Δ, which is illuminated by a ray parallel to a right section of the prism; the angle between the ray and the normal to the lateral face is Θ_i (Fig. 7.5). After two refractions, the incident ray dutifully emerges from the opposite face (provided that Θ_i is sufficiently large), having been deviated through a total angle θ relative to its original direction:

$$\theta = \Theta_i - \Theta_t + \Theta_t' - \Theta_i',$$

where $\sin\Theta_i = m\sin\Theta_t$, $\sin\Theta_t' = m\sin\Theta_i'$, and $\Theta_t' = \Delta - \Theta_t$. The deviation is an extremum for the angle of incidence where

$$\frac{d\theta}{d\Theta_i} = 1 - \frac{\cos\Theta_t'\cos\Theta_i}{\cos\Theta_t'\cos\Theta_t} = 0,$$

and by examining the sign of $d^2\theta/d\Theta_i^2$ we can show that the extremum is a minimum. The path of the minimally deviated ray is such that $\Theta_i = \Theta_t'$ and

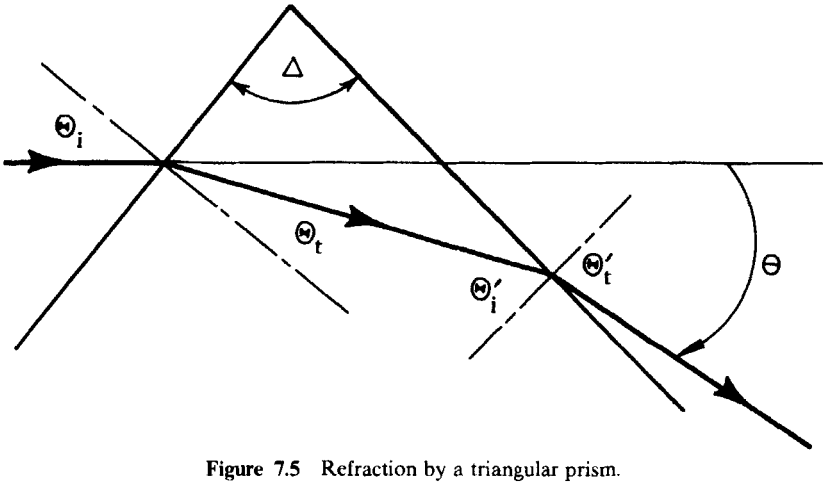

Figure 7.5 Refraction by a triangular prism.

$\Theta_t = \Theta_t'$; therefore, the angle of minimum deviation θ_m is

$$\theta_m = 2\sin^{-1}\left(m\sin\frac{\Delta}{2}\right) - \Delta. \tag{7.16}$$

By analogy with the primary rainbow angle—an angle of minimum deviation—we expect maxima (caustics) in the scattering diagrams of prismatic particles at angles given by (7.16). The crystallographic form of ice is hexagonal; therefore, hexagonal ice crystals occasionally inhabit the atmosphere. And if such crystals are interposed between the sun and an informed observer, haloes and a myriad of other optical displays may be seen.

There are two haloes that may be attributed to minimum angles of deviation associated with ice crystals: the 22° halo and the 46° halo, the former being the most common. But both are much more common than is generally realized; their frequency is a function of the state of awareness of the observer. To test this, one can ask a class of undergraduates—or an audience of Ph.D. physicists for that matter—if anyone has ever seen a halo or a sun dog. The response is likely to be feeble. But within a few days after explaining these phenomena, you are usually deluged with phone calls or confronted by breathless students all aglow from having seen what had previously been a "rare" phenomenon.

The angular positions of the two haloes can be determined from (7.16); the smaller halo is associated with a vertex angle of 60° and the larger with 90° (Fig. 7.6). Ice is slightly birefringent (Hobbs, 1974, p. 202), but we can ignore this and take $m = 1.318$ as the refractive index of "blue" light and $m = 1.308$ as that of "red" light. The corresponding angles of minimum deviation

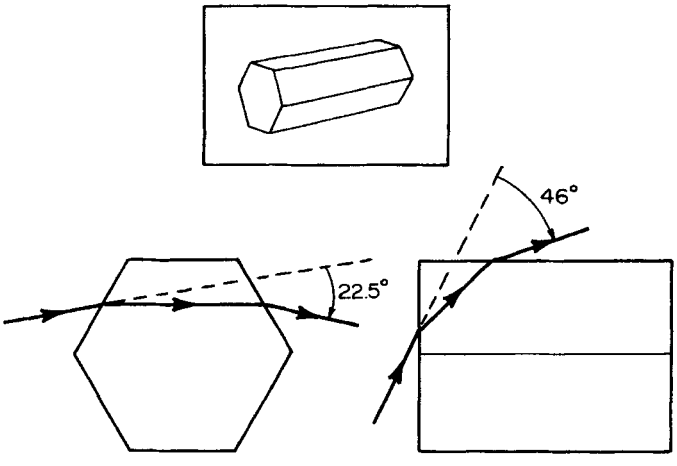

Figure 7.6 Refraction by a hexagonal ice crystal showing the rays associated with the 22° and 46° haloes.

calculated from (7.16) are

$$\begin{aligned} \theta_m(\text{blue}) &= 22.4°, \\ \theta_m(\text{red}) &= 21.7°, \end{aligned} \qquad \Delta = 60°$$

$$\begin{aligned} \theta_m(\text{blue}) &= 47.5°, \\ \theta_m(\text{red}) &= 45.3°, \end{aligned} \qquad \Delta = 90°.$$

Geometrical optics therefore correctly predicts the approximate angular positions of the two most commonly observed ice crystal haloes. Note that red light is deviated least, so the haloes may exhibit color separation with red appearing at their inner edges.

Complete haloes are traditionally attributed to scattering by randomly oriented ice crystals (but, see Fraser, 1979, for a contrary viewpoint); sun dogs or mock suns—brights spots on one or both sides of the sun, at about 22° when the sun is low—are the result of scattering by oriented crystals. This, however, by no means exhausts the list of atmospheric optical phenomena associated with ice crystals; there are many more, some of which are quite rare. But these are beyond the scope of this section, which is meant to be only a simple application of geometrical optics to light scattering by nonspherical particles. Suggestions for further reading are given below.

NOTES AND COMMENTS

Justification for dividing the light scattered by large particles into diffracted, reflected, and transmitted components is provided by the *localization principle* (van de Hulst, 1957, pp. 208–214) whereby the terms in the Mie series are associated with each of these components.

The quality of rainbow colors is not uniform across the bow; the reasons for this are given by Fraser (1972).

Neuberger (1951, p. 174) reports that halo phenomena were observed an average of 74 days a year over a 16-year period in State College, Pennsylvania. They are just as common on the other side of the Atlantic: near Bristol, England, Brain (1972) observed halo phenomena on 80 occasions in 66 days.

Haloes and other ice crystal phenomena are discussed by Minnaert (1954), Tricker (1970, 1979), and Greenler (1980). The book by the latter author is particularly recommended for its clarity and its superb color photographs.

The *Journal of the Optical Society of America* for August 1979 is almost entirely devoted to meteorological optics; it contains several papers on rainbows, the glory, and ice crystal phenomena.